

Simultaneously sorting overlapping quantum states of light

Suraj Goel,^{*} Max Tyler,^{*} Feng Zhu, Saroch Leedumrongwatthanakun, Mehul Malik, and Jonathan Leach[†]
School of Engineering and Physical Sciences, Heriot-Watt University, Edinburgh, EH14 4AS, UK

The efficient manipulation, sorting, and measurement of optical modes and single-photon states is fundamental to classical and quantum science. Here, we realise simultaneous and efficient sorting of non-orthogonal, overlapping states of light, encoded in the transverse spatial degree of freedom. We use a specifically designed multi-plane light converter (MPLC) to sort states encoded in dimensions ranging from $d = 3$ to $d = 7$. The MPLC simultaneously performs the unitary operation required for unambiguous discrimination and the basis change for the outcomes to be spatially separated.

Introduction:– The task of discriminating between a set of quantum states is a fundamental requirement in quantum information science, and in particular, quantum communication [1, 2]. However, as quantum states can be described as superpositions of one another, two different quantum states can have a finite, non-zero overlap with respect to each other, making them non-orthogonal and therefore difficult to separate. It is theoretically impossible to perform a measurement that allows us to distinguish such states 100% of the time. An important question now follows: given a set of quantum states with a non-zero overlap, what is the best measurement strategy to distinguish between them? For example: how do we optimally measure horizontal and diagonal polarization states; how would we separate Hermite-Gaussian modes from Laguerre-Gaussian modes; or how could we classify overlapping images?

The answer to these questions lies in quantum measurement theory, and there are known strategies for the optimal measurement of non-orthogonal quantum states [3, 4]. We are left with a choice between a measurement strategy that is either efficient OR accurate (only orthogonal states can sorted efficiently AND accurately). The efficient option is minimum error state discrimination (MESD) [5]. Here, one seeks to perform a set of measurements that categorises every input state. The drawback to MESD is that errors are inevitable, and we have to accept that we will be incorrect with some probability relating to the overlap of the input states. The accurate option is unambiguous state discrimination (USD) [6–8]. Here, one seeks to perform measurements that never incorrectly identify the input state. The downside here is that state identification occurs with a reduced probability, i.e. a measurement does not always provide a result, but when it does, it is always correct. The difference between MESD and USD is illustrated in Fig. 1. The first experimental realisation of unambiguous state discrimination was achieved for qubits in the polarisation degree of freedom [9], which was achieved using a set of wave-plates and polarization beam-splitters.

The problem that we address in this work is practical high-dimensional unambiguous state discrimination, i.e. a positive operator-valued measure (POVM) for high-dimensional non-orthogonal states. High-dimensional

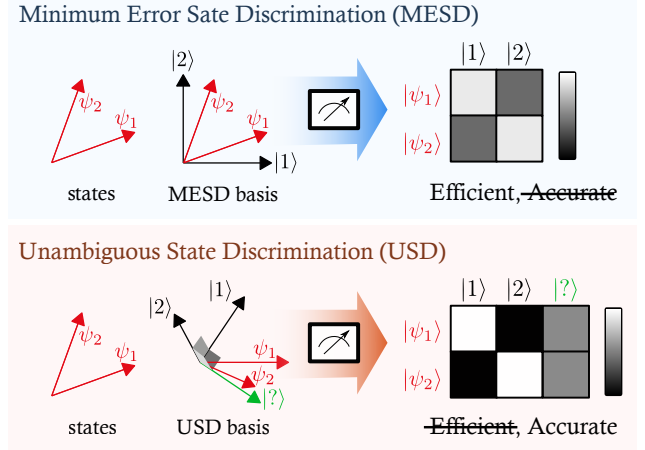


FIG. 1. Measuring non-orthogonal states using minimum error or unambiguous state discrimination. The MESD protocol is efficient in that every input state is always categorised, even if this leads to errors. The USD protocol is accurate in that every input state is correctly identified, even if this does not happen 100% of the time.

states allow for quantum information to be encoded in a d -dimensional space, known as qudits, and they are known to be robust to noise [10–12]. While the theoretical foundation to the necessary measurement strategies has already been developed, their experimental realisation has provided a significant challenge. This is because in order to perform unambiguous state discrimination, one needs a device that can perform a unitary operation within the Hilbert space, while simultaneously sorting the outcomes onto individual detectors.

Unambiguous state discrimination was simulated for single-photon states of light encoded in high dimensions [13]. However, due to lack of a high-dimensional sorting device, the states were separated sequentially using single-outcome projective measurements. Such single-outcome projective measurements compromise their use in quantum communication where multi-outcome measurements are paramount, as well as in the field of quantum foundations, where fair-sampling requires that all possible states are measured simultaneously [14]. Thus, developing systems for the efficient sort-

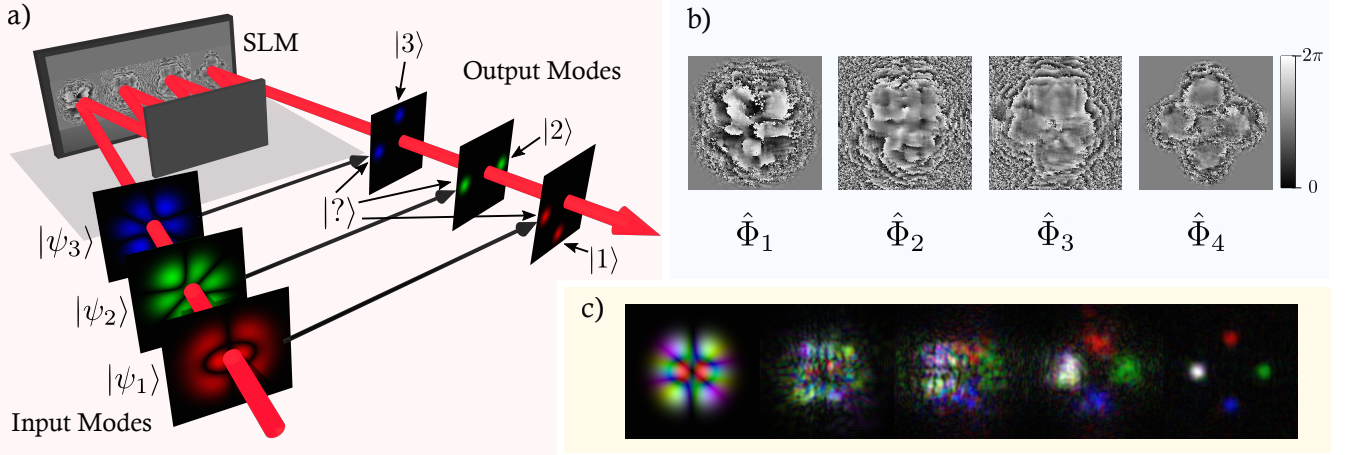


FIG. 2. (a) Schematic of the mode sorter for non-orthogonal states with colour used to represent different input modes. The d input modes pass through a multi-plane light converter that sorts them into $d + 1$ orthogonal outputs of spatially separated Gaussian spots. The one additional output mode $|?\rangle$ corresponds to the ambiguous outcome. (b) Example holograms used for the MPLC. (c) Amplitudes of non-orthogonal modes as they propagate through the MPLC.

ing of high-dimensional states is an important challenge and key to realising their full potential. Recent work on state discrimination includes that on high-dimensional states using optimal measurement strategies [15], multi-state quantum discrimination through optical networks [16], and quantum state elimination [17]. Additionally, much of recent this work resembles the goals of the complementary field of classical deep optical networks used for information processing and image classification using diffractive optics [18–20].

Due to the limitations of single-outcome projective measurements, methods for sorting states rather than sequentially measuring them have been the topic of significant recent research [21–27]. Here, the goal is to take d orthogonal input modes in a particular basis and map them to d orthogonal output modes that are easily measured, for example by a camera, a single-photon detector array, or an array of fibres connected to detectors. Such a system can operate with 100% efficiency in principle, which is normally reduced by practical considerations relating to the devices used. Two phase screens can be used to convert modes with orbital angular momentum to position modes of light [22, 23]. More recently, general unitary operations have been made possible in multi-mode fibers [28] or in free-space using multi-plane light converters (MPLC) [24–26]. These devices use multiple phase screens to transform and measure complete sets of orthogonal modes, e.g. Hermite-Gaussian and Laguerre-Gaussian modes [27] and implement quantum gates for high-dimensional modes of light [28–31]. Extension to cover the transformations over polarization spatio-temporal optical fields has been demonstrated recently [32].

The problem we set out to solve in this work is

the simultaneous sorting of d equally overlapping d -dimensional quantum states of light $\{|\psi_1\rangle, \dots, |\psi_d\rangle\}$ with fidelities given by $F = |\langle\psi_i|\psi_{j\neq i}\rangle|^2$ [33]. States that are orthogonal have a fidelity of $F = 0$ with respect to each other; states that are collinear have a fidelity of $F = 1$.

There are several requirements that must be met in order to achieve the goal of sorting non-orthogonal states. Our first requirement is that every input mode in the set $\{|\psi_1\rangle, \dots, |\psi_d\rangle\}$ is mapped to an individual measurement mode $\{|1\rangle, \dots, |d\rangle\}$ that uniquely identifies it, i.e. when a photon in state $|\psi_1\rangle$ passes through the system, only the measurement mode $|1\rangle$ can “click.” The challenge is to perform this sorting when every state in the set has a non-zero fidelity with respect to every other state in the set, i.e. $0 < |\langle\psi_i|\psi_{j\neq i}\rangle|^2 < 1$. Our second requirement is that the system should not make any errors and incorrectly identify any input state, i.e. for the $|\psi_1\rangle$ input state, the probability of all output modes other than $|1\rangle$ clicking should be equal to zero. The final requirement is that the sorting process occurs simultaneously, and with the highest possible efficiency. This efficiency is given by $\eta = 1 - |\langle\psi_i|\psi_{j\neq i}\rangle|^2$ when all states in the set have an equal fidelity with every other state. The work reported here shows that we can experimentally achieve all of these requirements on the same device with an appropriately designed MPLC.

MPLC for USD:– The key to our sorting method is to realise unambiguous state discrimination within the framework of a multi-plane light converter (MPLC), as shown in Fig. 2. This allows us to simultaneously transform a set of non-orthogonal states in any basis into a new basis of spatially separated measurement modes that can be simultaneously detected by a position-resolving detector. Here, we design the output modes of the MPLC to be

spatially separated Gaussian spots that can be directly read by a camera or a single-photon detector array. The MPLC is trained to perform the required unitary (USD operation) and the necessary mode conversion (HG \rightarrow Gaussian spots) at the same time.

The holograms used in MPLC devices are typically designed using a process known as wavefront matching [26, 27, 34, 35]. This is an iterative procedure where the optical fields for the input modes and the output modes are forward and backward propagated to the planes of the MPLC. The phase of the MPLC at each plane is calculated in such a way that the entire set of input modes are phase-matched to the respective output modes. This process is repeated for each plane sequentially until the algorithm converges and the difference between the forward and backwards propagating light is minimised. As noted in [26] and [27], a mode sorter performs well when the difference between these two sets of modes (input and output) is minimised.

Here we introduce an additional output state, labelled $|?\rangle$, into the wavefront matching protocol, which means that for d input modes, there are $d+1$ output modes. The purpose of the $|?\rangle$ output is that if a photon is detected in this mode, it provides no information about the input state. However, this also implies that we have not made any incorrect identification, as required by USD. As we can successfully discriminate between two states with a probability of $1-F$, the probability that $|?\rangle$ clicks is equal to F .

The MPLC uses multiple addressable phase masks combined with free-space propagation to approximate arbitrary unitary transformations [24–27]. Each reflection from a mask performs a phase-only transformation $\hat{\Phi}_i$ of the input states of light, which is followed by free-space propagation to the next plane \hat{H} . The total operator of the device after n reflections is given by $\hat{U} = \hat{H} \prod_{i=n}^1 (\hat{\Phi}_i \hat{H})$.

The key to the success of this work is that this operator is designed to perform both a unitary operation that maps a set of input states onto the required unambiguous measurement states and simultaneously change the basis for the measurement outcomes to be spatially separated. All of this is performed concurrently within the MPLC.

Results:— We performed unambiguous state discrimination for sets of symmetric non-orthogonal states constructed from modes in the Hermite-Gaussian (HG) basis. We perform this experiment with a HeNe laser and detect with a CMOS camera. Although this experiment was performed with coherent states of light, the theoretical formalism still applies at the single-photon level.

In each realisation of USD for high-dimensional states of light, d non-orthogonal modes were transformed into $d+1$ output modes and measured simultaneously on a CMOS camera. The intensities recorded by the camera pixels located in the output modes were integrated and

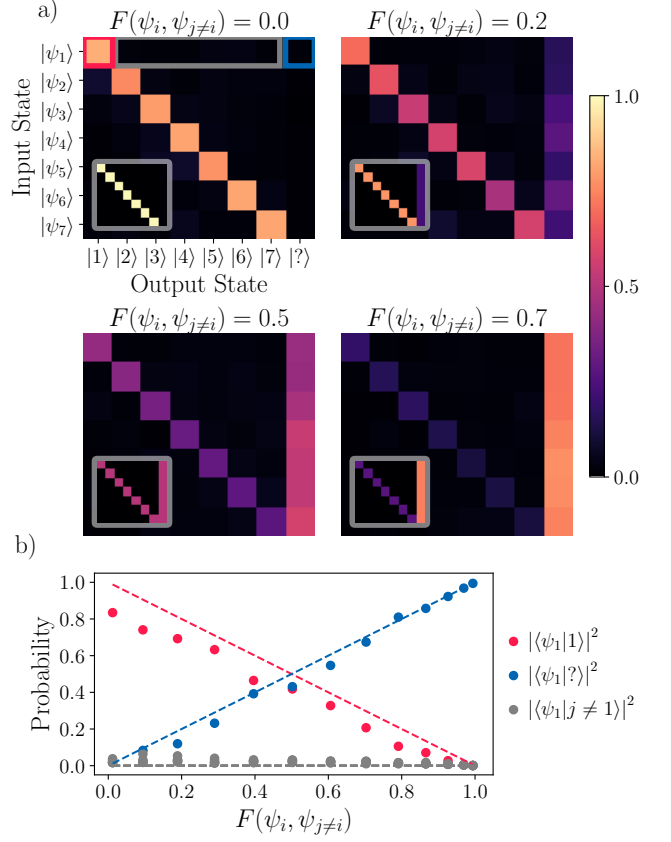


FIG. 3. Measurement data for simultaneous USD in $d = 7$ using an MPLC. (a) Measurement matrices for a range of fidelities (F) between the input states. The insets show the numerically modelled results. The results are normalised by the total power detected in each output mode. (b) Probability of measuring a value in the given output mode $|x\rangle$ given the input mode $|\psi_1\rangle$ as a function of inter-state fidelity. The points are the measured values, and the solid lines are the expected results. This is a cross section of the measurement matrices for the $|\psi_1\rangle$ input state.

converted to a detection probability. We achieved USD for sets of states in dimensions from $d = 3$ to 7 for fidelities in the range $F(\psi_i, \psi_j \neq i) \in (0, 1)$. Each state is generated as a complex superposition of Hermite - Gauss basis modes while varying the fidelity from 0 to 1, (see Supplementary Information for further details). The results for USD in 7 dimensions are displayed in Fig. 3.

To quantitatively assess our system, we analyse the performance of the MPLC compared to the theoretical limit of minimum error state discrimination (MESD) [13, 36]. In MESD in d dimensions no auxiliary state is used, and the error is instead distributed between the d output states. This leads to a probability of error (p_{err}) in the output, which is defined as the probability of measuring any output state $|j \neq i\rangle$ when given an input state $|\psi_i\rangle$. MESD for uniform-fidelity states has a minimum possible error probability given by: $p_{\text{err}} \geq$

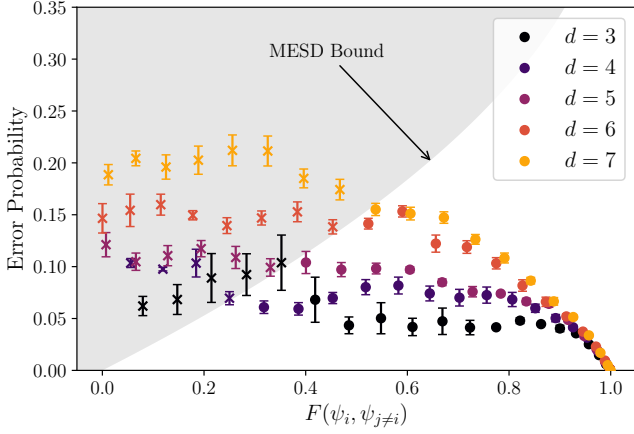


FIG. 4. Evaluation of the MPLC for USD compared to the theoretical limit of MESD. The grey shaded area indicates the area accessible via MESD; points below this region represent USD with an error rate that is below what is possible with MESD.

$$\frac{1}{2} \left(1 - \sqrt{1 - F(\psi_i, \psi_{j \neq i})} \right) \quad [13, 36].$$

In Fig. 4, we plot the error probabilities of our USD transformations against the MESD threshold (the grey area). We see that our system outperforms MESD and has a lower error rate than any strategy using MESD over a wide range of fidelities. The error probabilities are higher for lower F because the MPLC struggles more when sorting states that are farther apart. Additionally, as d increases, so too does the total error. The performance of the MPLCs reducing as d increases can be explained as the accuracy of the transformation is known to reduce as the dimensionality increases for a fixed number of phase planes [28]. Here we use a fixed number of four phase plane while increasing the dimensionality of the set of modes that we are sorting.

Theoretically, this error should be equal to zero for USD, yet we see the experimental implementation using the MPLC performs better for states with a higher initial fidelity. The reason for this is that as F increases, a higher fraction of the energy is put into the single ambiguous outcome. This mapping, where all input states are sorted to a single output state, is a simpler task to achieve for the MPLC than the case where all input states are sorted to individual outcomes. The extreme case is where $F = 1$, corresponding to all input states being equal, and these being mapped to a single outcome. In the limit that $F = 1$, this is a one-dimensional transformation and is accurately achieved by the MPLC, as discussed above.

Figure 5 shows the extension of our method to the sorting of overlapping images. The images that we sort are ones depicting a smiley face, sad face, and neutral face that have a large fidelity ($F = 0.34$) with respect to each other—the eyes in the images are the same, while

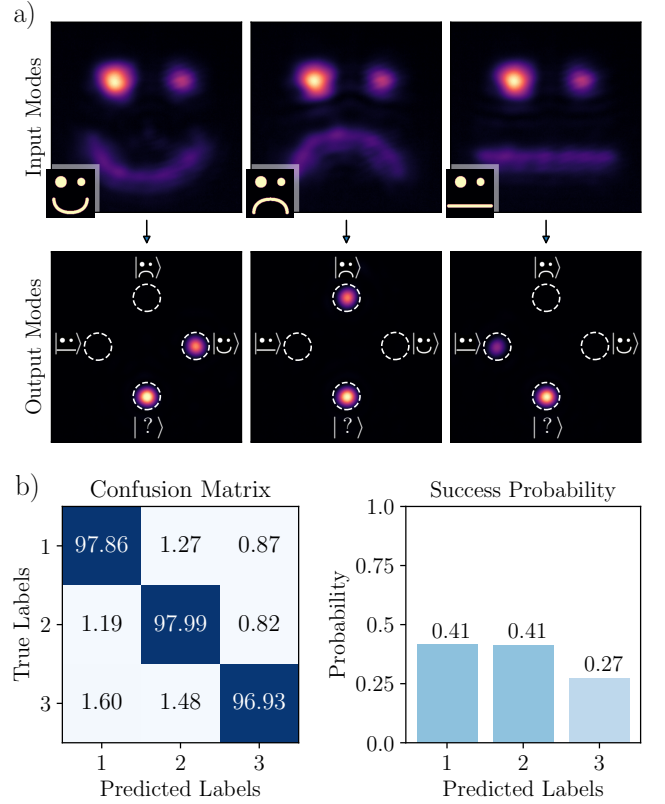


FIG. 5. Sorting overlapping images with the MPLC. The input images have a large fidelity ($F = 0.34$) with each other, yet we can sort them with an accuracy of 97.6%.

the mouth expressions are slightly different, connoting completely different emotions.

In a naive method of optical image classification, the three faces are transformed directly to three spatially separated spots, and the wavefront matching algorithm attempts to direct all input light into all output modes, leading to noisy classification. When using the extra mode $|?\rangle$, we have a place to direct any overlapping light, leading to potentially no noise in our measurement state outputs. Despite the large fidelity between the input images, we are able to effectively sort and classify with an average accuracy of 97.6%.

Conclusions:— In general, two quantum states will not necessarily be orthogonal with respect to each other. This poses a significant challenge with regards to their optimal measurement. In this work we solve this measurement problem, enabling the sorting of a set of non-orthogonal states of light. We show that the addition of an auxiliary measurement mode enables near-perfect sorting of non-orthogonal states of light. This work corresponds to the first positive operator-valued measure (POVM) for high-dimensional non-orthogonal states of light, extending the use of MPLCs to include non-orthogonal input modes.

The key to success is the additional output mode that provides extra flexibility to the system and enables perfect mapping from every d non-orthogonal input states to a unique output. The only price that we pay is that there is a reduction in success probability of the mapping due to the non-orthogonality of the input states. We have traded efficiency for accuracy, but the method we adopt is the optimal strategy for minimising errors and correctly identifying images. The consequence is that at the single-photon level, the sorting does not provide an outcome 100% of the time, and for intense modes of light, there is a reduction in the total power that is transmitted into the known output modes. Future work will focus on extending our method to sort quantum states and modes that have a non-uniform fidelity with respect to each other.

Acknowledgements:—We thank Will McCutcheon for fruitful discussions regarding this work. This work was supported by EPSRC grants EP/T00097X/1 and EP/P024114/1, by QuantERA ERA-NET Co-fund (FWF Project I3773-N36), and the European Research Council (ERC) Starting grant PIQUaNT (950402).

* These authors contributed equally

† j.leach@hw.ac.uk

- [1] C. W. Helstrom, *Journal of Statistical Physics* **1**, 231 (1969).
- [2] M. A. Nielsen and I. L. Chuang, *Quantum Computation and Quantum Information: 10th Anniversary Edition* (Cambridge University Press, 2010).
- [3] S. M. Barnett and S. Croke, *Adv. Opt. Photon.* **1**, 238 (2009), [arxiv:0810.1970](#).
- [4] A. Chefles, *Contemporary Physics* **41**, 401 (2000).
- [5] S. M. Barnett and S. Croke, *Journal of Physics A: Mathematical and Theoretical* **42**, 062001 (2009).
- [6] I. Ivanovic, *Physics Letters A* **123**, 257 (1987).
- [7] A. Chefles and S. M. Barnett, *Physics Letters A* **250**, 223 (1998).
- [8] A. Chefles, *Physics Letters A* **239**, 339 (1998).
- [9] R. B. M. Clarke, A. Chefles, S. M. Barnett, and E. Riis, *Phys. Rev. A* **63**, 040305 (2001), [arxiv:quant-ph/0007063](#).
- [10] F. Zhu, M. Tyler, N. H. Valencia, M. Malik, and J. Leach, *AVS Quantum Science* **3**, 011401 (2021), [arXiv:1908.08943](#).
- [11] S. Ecker, F. Bouchard, L. Bulla, F. Brandt, O. Kohout, F. Steinlechner, R. Fickler, M. Malik, Y. Guryanova, R. Ursin, and M. Huber, *Phys. Rev. X* **9**, 041042 (2019), [arXiv:1904.01552](#).
- [12] V. Srivastav, N. H. Valencia, W. McCutcheon, S. Leedumrongwatthanakun, S. Designolle, R. Uola, N. Brunner, and M. Malik, (2022), [arXiv:2202.09294](#).
- [13] M. Agnew, E. Bolduc, K. J. Resch, S. Franke-Arnold, and J. Leach, *Phys. Rev. Lett.* **113**, 020501 (2014), [arXiv:1403.3830](#).
- [14] B. G. Christensen, K. T. McCusker, J. B. Altepeter, B. Calkins, T. Gerrits, A. E. Lita, A. Miller, L. K. Shalm, Y. Zhang, S. W. Nam, N. Brunner, C. C. W. Lim, N. Gisin, and P. G. Kwiat, *Phys. Rev. Lett.* **111**, 130406 (2013), [arXiv:1306.5772](#).
- [15] M. Solís-Prosser, O. Jiménez, A. Delgado, and L. Neves, *Quantum Science and Technology* **7**, 015017 (2021).
- [16] A. Laneve, A. Gerdali, F. Hamiti, P. Mataloni, and F. Caruso, *Quantum Science and Technology* **7**, 025028 (2022), [arXiv:2107.09968](#).
- [17] J. W. Webb, I. V. Puthoor, J. Ho, J. Crickmore, E. Blakely, A. Fedrizzi, and E. Andersson, (2022), [arXiv:2207.00019](#).
- [18] X. Lin, Y. Rivenson, N. T. Yardimci, M. Veli, Y. Luo, M. Jarrahi, and A. Ozcan, *Science* **361**, 1004 (2018), [arXiv:1804.08711](#).
- [19] G. Wetzstein, A. Ozcan, S. Gigan, S. Fan, D. Englund, M. Soljačić, C. Denz, D. A. B. Miller, and D. Psaltis, *Nature* **588**, 39 (2020).
- [20] O. Kulce, D. Mengu, Y. Rivenson, and A. Ozcan, *Light: Science & Applications* **10**, 1 (2021), [arXiv:2007.12813](#).
- [21] J. Leach, M. J. Padgett, S. M. Barnett, S. Franke-Arnold, and J. Courtial, *Phys. Rev. Lett.* **88**, 257901 (2002).
- [22] G. C. G. Berkhout, M. P. J. Lavery, J. Courtial, M. W. Beijersbergen, and M. J. Padgett, *Phys. Rev. Lett.* **105**, 153601 (2010).
- [23] M. Mirhosseini, M. Malik, Z. Shi, and R. W. Boyd, *Nature Communications* **4**, 2781 (2013), [arXiv:1306.0849](#).
- [24] J. F. Morizur, L. Nicholls, P. Jian, S. Armstrong, N. Treps, B. Hage, M. Hsu, W. Bowen, J. Janousek, and H. A. Bachor, *Journal of the Optical Society of America A* **27**, 2524 (2010), [arXiv:1005.3366](#).
- [25] G. Labroille, B. Denolle, P. Jian, P. Genevieux, N. Treps, J. F. Morizur, P. Genevieux, and N. Treps, *Optics Express* **22**, 15599 (2014), [arXiv:1404.6455](#).
- [26] N. K. Fontaine, R. Ryf, H. Chen, D. Neilson, and J. Carpenter, in *2017 European Conference on Optical Communication (ECOC)* (2017) pp. 1–3.
- [27] N. K. Fontaine, R. Ryf, H. Chen, D. T. Neilson, K. Kim, and J. Carpenter, *Nature Communications* **10**, 1865 (2019), [arXiv:1803.04126](#).
- [28] S. Goel, S. Leedumrongwatthanakun, N. H. Valencia, W. McCutcheon, C. Conti, P. W. Pinkse, and M. Malik, (2022), [arXiv:2204.00578](#).
- [29] F. Brandt, M. Hiekkamäki, F. Bouchard, M. Huber, and R. Fickler, *Optica* **7**, 98 (2020), [arXiv:1907.13002](#).
- [30] M. Hiekkamäki and R. Fickler, *Physical Review Letters* **126**, 123601 (2021), [arXiv:2006.13288](#).
- [31] O. Lib, K. Sulimany, and Y. Bromberg, (2021), [arXiv:2108.02258](#).
- [32] M. Mounaix, N. K. Fontaine, D. T. Neilson, R. Ryf, H. Chen, J. C. Alvarado-Zacarias, and J. Carpenter, *Nature Communications* **11**, 5813 (2020), [arXiv:1909.07003](#).
- [33] S. Franke-Arnold and J. Jeffers, *The European Physical Journal D* **66**, 196 (2012).
- [34] T. Hashimoto, T. Saida, I. Ogawa, M. Kohtoku, T. Shibata, and H. Takahashi, *Optics Letters* **30**, 2620 (2005).
- [35] Y. Sakamaki, T. Saida, T. Hashimoto, and H. Takahashi, *J. Lightwave Technol.* **25**, 3511 (2007).
- [36] D. Qiu, *Phys. Rev. A* **77**, 012328 (2008), [arXiv:0707.3970](#).
- [37] V. Arrizón, G. Méndez, and D. S. de La-Llave, *Opt. Express* **13**, 7913 (2005).

Supplementary Material : Simultaneously sorting overlapping quantum states of light

Unambiguous State Discrimination:— In the process of unambiguous state discrimination (USD), our task is to accurately identify a random state from a set of states $S = \{|\psi_i\rangle\}_i$. In general, this set of states S are non-orthogonal with each other. If two states have an overlap along a vector, when a state measurement collapses into this vector, we get no information of which state we started with. Since this measurement needs to be accurate, we denote this outcome as an ambiguous outcome. Alternatively if the result of the collapse is a vector which only has overlap with one of our initial states, then we can be sure that was the state we started with. The vectors we measure with are denoted $|i\rangle$ for the state which only has overlap with $|\psi_i\rangle$ and $|?_j\rangle$ for the state with multiple non-zero overlaps. This set of states forms a projective operator-valued measure (POVM). In general, there could be different overlaps between different states in S corresponding to different ambiguous outcomes $|?_j\rangle$, however in this work we looked at symmetric states which have equal overlap with each other corresponding to a single ambiguous outcome denoted by $|?\rangle$.

Generation of symmetric states:— A set of d d -dimensional symmetric states $\{|\psi_i\rangle\}_i$ is defined such that $|\langle\psi_i|\psi_j\rangle|^2 = \delta_{ij} + (1 - \delta_{ij})|\beta|^2$, where β is the overlap between any two different states in the set. To be able to perform our USD measurements, we need a set of orthogonal measurement states ($|i\rangle$ and $|?\rangle$). To find these, we first construct the set of states $\{|i\rangle\}_i$ where $|i\rangle$ is orthogonal to every state but $|\psi_i\rangle$ ($\langle i|\psi_j\rangle = \delta_{ij}\alpha$). These states form an orthogonal basis for the initial set of states in d dimensions. We then increase the dimension of the space to $d' = d + 1$ by adding in an extra basis element $|?\rangle$ which is orthogonal to every $|i\rangle$. We now only need to find the transformation \hat{V} which takes $|\psi_i\rangle$ ($= \sum_j \psi_{ij} |j\rangle = \alpha |i\rangle + \sum_{j \neq i} \psi_{ij} |j\rangle$) to $|\psi'_i\rangle = \hat{V} |\psi_i\rangle = \alpha |i\rangle + \beta |?\rangle$.

For this experiment, we constructed a set of states with a parameter θ which allowed us to control the fidelity. We start by building a set of d ($d-1$)-dimensional states with overlap:

$$\langle \psi'_i | \psi'_j \rangle = -\frac{1}{d-1} \quad (\text{S.1})$$

These are generated with an iterative technique similar to Gram-Schmidt orthonormalisation. To generate the set of d vectors $\{|\psi_i\rangle\}_i$ in $d-1$ dimensions: Let ψ_i^j be the j 'th component of the i 'th vector.

Find the components as:

$$\psi_i^j = \begin{cases} 1, & \text{when } i = j = 1 \\ \frac{-\frac{1}{d-1} - \sum_{a < j} \psi_i^a \psi_j^{*a}}{\psi_j^j}, & \text{when } j < i \text{ or } j+1 = i = d \\ \sqrt{1 - \sum_{a < j} \psi_i^a \psi_i^{*a}}, & \text{when } j = i \\ 0, & \text{otherwise} \end{cases} \quad (\text{S.2})$$

Once these states are made, we mix them into the additional dimension by:

$$|\psi_i\rangle = \sin(\theta) |\psi'_i\rangle + \cos(\theta) |d\rangle \quad (\text{S.3})$$

Experimentally, we generate each state $|\psi_i\rangle$ as a superposition of Hermite-Gauss modes with the vectors computed following the algorithm above. For a given dimension d , we choose HG modes as the basis which follow the relation $n + m + 1 = d$, where m and n are number of nodes in either direction.

Sorting non-orthogonal states:— In order to perform USD measurements on these set of d d -dimensional symmetric states $S = \{|\psi_i\rangle\}_i$, we need to define a set of measurement states. To do so, first calculate $|\psi_i^\perp\rangle$, which are orthogonal to every state but $|\psi_i\rangle$. This can be done by taking the SVD of all the $|\psi_{j \neq i}\rangle$ stacked as a matrix, and removing the components of $|\psi\rangle$ from the subspace this matrix spans. We then define the set of measurement states $\{D_i\}$ by expanding the Hilbert-space into a higher dimension using $|\psi_{d+1}\rangle$ which is orthogonal to every state in S as

$$D_i = |\psi_i^\perp\rangle + \sqrt{-\langle \psi_1^\perp | \psi_2^\perp \rangle} |d+1\rangle \quad (\text{S.4})$$

and then normalise it. The overlap $\langle \psi_i^\perp | \psi_j^\perp \rangle = \langle \psi_1^\perp | \psi_2^\perp \rangle$ is the same for any two states $i \neq j$. The unknown state is included by Gram-Schmidt orthogonalisation with this set of states. We also need to extend our original states $|\psi_i\rangle$ into this space, and we do this just by adding the extra basis element $|\psi_{d+1}\rangle$ with 0 as its coefficient.

The final sorting is achieved using multi-plane light conversion that converts the set of states $\{D_i\}$ into spatially separated outcomes on a camera.

Multi Plane Light Conversion:— The multi-plane light converter (shown in Fig. S.1) is a device which is trained to do a specific transformation on input light. It is formed of multiple planes in series which each impart a phase change on the light-field, and this phase change combined with the propagation of light between planes can approximate unitary transformations on the input light.

Plane i performs a phase-only transformation $\hat{\Phi}_i$ to the light, which is followed by propagation to the next plane \hat{H} , giving the matrix of the device: $\hat{U} = \hat{H} \prod_{i=n}^1 (\hat{\Phi}_i \hat{H})$.

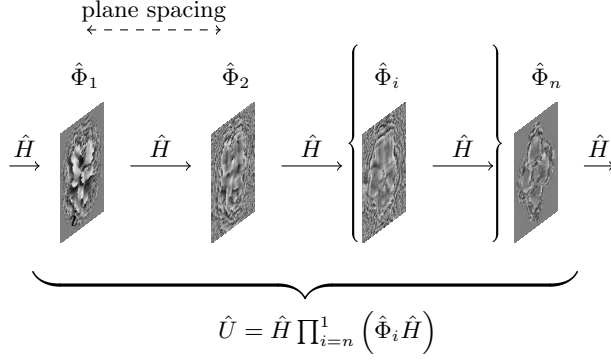


FIG. S.1. Illustrative diagram of MPLC: The unitary operation given as a product of multiple free-space propagation operators and phase planes.

The calculation of the masks is done with the wavefront matching method.

Simulation of Light Propagation:— To simulate light propagation, we use the approximation of a 3-dimensional scalar field $\psi(\mathbf{x})$, and define an initial field over a plane P orthogonal to the light's main propagation direction $\hat{\mathbf{n}}$: $P = \{\mathbf{x} \mid (\mathbf{x} - \mathbf{a}) \cdot \hat{\mathbf{n}} = 0\}$. The field is then propagated a distance α along the vector $\hat{\mathbf{n}}$ by the operator $e^{-i\hat{H}\alpha}$ to give its value for all points \mathbf{x} .

To approximate this calculation on the computer, we first discretise the field $\psi(\mathbf{x})$ over the plane P into the

vector ψ_{ij} , where the indices i and j index two orthogonal directions. We take the Fourier transform of this vector in both of these indices to give $\tilde{\psi} = \mathcal{F}(\psi)$. The phase change over a distance α along the $\hat{\mathbf{n}}$ direction for light of spatial frequency $|k| = \frac{2\pi}{\lambda}$ is given by:

$$\exp(-ik_{\hat{\mathbf{n}}}\alpha) = \exp\left(-i\sqrt{\left(\frac{2\pi}{\lambda}\right)^2 - |k_{\perp\hat{\mathbf{n}}}|^2}\alpha\right) \quad (\text{S.5})$$

Where the value $|k_{\perp\hat{\mathbf{n}}}|^2$ is sum of the squares of the coordinates $\tilde{\psi}$ is defined over. The inverse Fourier transform is then taken of this product to get the field at the new plane $\alpha\hat{\mathbf{n}}$ from the initial:

$$\psi(\alpha) = \mathcal{F}^{-1}\{\exp(-ik_{\hat{\mathbf{n}}}\alpha)\mathcal{F}(\psi_0)\} \quad (\text{S.6})$$

Wavefront Matching:— In order to encode a transformation within an MPLC, we need to calculate the right patterns to be displayed on each plane. This is done by a process called “wavefront matching”. It consists of propagating the input modes forward through the planes, and the output modes backward through the planes. At the plane where the modes meet, we create a new mask as the average overlap over all modes.

If our input modes at plane p are $a_{i,p}(x)$, and our output modes are $b_{i,p}(x)$ then the expression for the next plane mask is given by:

$$\Phi'_p(x) = \sum_i a_{i,p}(x)b_{i,p}^*(x) \exp\left(-i \arg\left[\int dx \Phi_p^*(x)a_{i,p}(x)b_{i,p}^*(x)\right]\right) \quad (\text{S.7})$$

The forward, and backward propagating fields at plane p are given by $a_{i,p}(x)$ and $b_{i,p}(x)$ respectively. The goal is to have the fields exactly matching at those points, so that $\langle a_{i,p} | \Phi_p^\dagger | b_{i,p} \rangle = 1$ over all input modes i . The change

in the phase mask can be written in terms of its phase:

$$\Phi'(x) = e^{i(\theta(x) + \delta\theta(x))} \quad (\text{S.8})$$

$$\approx e^{i\theta(x)} (1 + i\delta\theta(x)) \quad (\text{S.9})$$

$$= \Phi(x) (1 + i\delta\theta(x)) \quad (\text{S.10})$$

The new overlap is given by:

$$\langle a_{i,p} | \Phi'^\dagger | b_{i,p} \rangle \quad (\text{S.11})$$

We want the new Φ' to increase the overlap:

$$\eta' = |\langle a_{i,p} | \Phi^\dagger | b_{i,p} \rangle|^2 \quad (\text{S.12})$$

$$\approx |\langle a_{i,p} | \Phi^\dagger (1 - i\delta\theta^\dagger) | b_{i,p} \rangle|^2 \quad (\text{S.13})$$

$$= |\langle a_{i,p} | \Phi^\dagger | b_{i,p} \rangle - i \langle a_{i,p} | \Phi^\dagger \delta\theta^\dagger | b_{i,p} \rangle|^2 \quad (\text{S.14})$$

$$= (\langle a_{i,p} | \Phi^\dagger | b_{i,p} \rangle - i \langle a_{i,p} | \Phi^\dagger \delta\theta^\dagger | b_{i,p} \rangle) \overline{(\langle a_{i,p} | \Phi^\dagger | b_{i,p} \rangle - i \langle a_{i,p} | \Phi^\dagger \delta\theta^\dagger | b_{i,p} \rangle)} \quad (\text{S.15})$$

$$= \eta + 2\Re \left\{ i \langle a_{i,p} | \Phi^\dagger | b_{i,p} \rangle \overline{\langle a_{i,p} | \Phi^\dagger \delta\theta^\dagger | b_{i,p} \rangle} \right\} + \mathcal{O}(\delta\theta^2) \quad (\text{S.16})$$

$$\approx \eta - 2\Im \left\{ \langle a_{i,p} | \Phi^\dagger | b_{i,p} \rangle \overline{\langle a_{i,p} | \Phi^\dagger \delta\theta^\dagger | b_{i,p} \rangle} \right\} \quad (\text{S.17})$$

And so to satisfy $\eta' > \eta$, we just need:

$$\Im \left\{ \langle a_{i,p} | \Phi^\dagger | b_{i,p} \rangle \overline{\langle a_{i,p} | \Phi^\dagger \delta\theta^\dagger | b_{i,p} \rangle} \right\} < 0 \quad (\text{S.18})$$

We let $\alpha = \langle a_{i,p} | \Phi^\dagger | b_{i,p} \rangle$, and separate $\overline{\langle a_{i,p} | \Phi^\dagger \delta\theta^\dagger | b_{i,p} \rangle}$ into its components, requiring the inequality to be satisfied for each individual component:

$$\Im \left\{ \alpha a_{i,p}(x) e^{i\theta(x)} \delta\theta(x) b_{i,p}^\dagger(x) \right\} < 0 \quad (\text{S.19})$$

And letting $\gamma(x) = \alpha a_{i,p}(x) e^{i\theta(x)} b_{i,p}^\dagger(x)$:

$$\delta\theta(x) \Im \{ \gamma(x) \} < 0 \quad (\text{S.20})$$

By letting $\delta\theta(x) = -\Im \{ \gamma(x) \}$, we can satisfy this equation. So, to update the phase mask:

$$\Phi'(x) = \sum_i e^{i\theta(x)} e^{-i\Im \{ \langle a_{i,p} | \Phi^\dagger | b_{i,p} \rangle a_{i,p}(x) e^{i\theta(x)} b_{i,p}^\dagger(x) \}} \quad (\text{S.21})$$

Experimental Setup:— As illustrated in Fig. S.2, the experimental setup consists of three sections: generation, conversion and measurement. The desired non-orthogonal states are generated at a first SLM are then unambiguously discriminated at the second SLM, which acts as a multi-plane light converter (MPLC). The intensity distribution of the output states are then measured using a camera.

For the generation of the input states, we first use a 5 mW He-Ne Laser to produce a linearly polarized beam at 633 nm. This is then passed through a single-mode fiber and is collimated with a pair of lenses with focal lengths 45 mm and 100 mm. This beam then passes through a half-wave plate (HWP) such that it is polarized in the optical axis of the generation SLM (Holoeye Pluto 2.1). Our input modes are generated using computer generated holograms (CGH), which are calculated using the type 3 method as detailed in [37]. This beam is imaged to the input plane of the MPLC using two lenses of focal length 750 mm and 500 mm. We use a Fourier filter at the focus of the 750 mm lens to select generated beams.

The MPLC is build in the reflection mode with 4 phase planes comprising of a phase-only SLM (Meadowlark

E19x12) and a mirror, separated by 17 mm. Inside the MPLC, light undergo a transformation due to multiple reflection from the SLM followed by free-space propagation. Each reflection within the MPLC changes the phase profile of the mode. A grating of 10-pixel period is displayed across the whole SLM in order to efficiently separate modulated light from the residual. The target input and output modes are assigned at 17 mm propagation distance before the first and after the last reflection from the SLM.

Finally, the intensity distributions of the output modes are measured via the CMOS Camera (Thorlabs USB3.0) using a 4- f system with a focal length of 250 mm. Since our beam is reflected through the same grating 4 times, at the focal plane of this imaging system, we filter the 4th order diffraction that carries the fully transformed modes.

Data Processing:— We measure the experimental coupling matrices between the set of input modes and the output modes by measuring the intensity on each Gaussian spot. There are discrepancies between the ideal and measured intensities. This is due to a variety of factors like mode-dependent loss, imperfect wavefront matching, misalignments and subnormalised input state generation using computer-generated holograms (CGH).

We correct for these imperfections by multiplying the measured matrices with a “correction vector”. Experimentally, this can be interpreted as applying a non-uniform attenuation to different output modes. If our ideal USD matrix is M , and our experimentally measured USD matrix is E , we can construct a correction vector \mathbf{v} with elements:

$$\mathbf{v} = \left(\frac{E_{11}}{M_{11}} \quad \frac{E_{22}}{M_{22}} \quad \cdots \quad \frac{E_{dd}}{M_{dd}} \quad \frac{\sum_{i=1}^d E_{i(d+1)}}{\sum_{i=1}^d M_{i(d+1)}} \right) \quad (\text{S.22})$$

Which can correct our measurements by multiplying column-wise:

$$M'_{ij} = M_{ij} \mathbf{v}_j \quad (\text{S.23})$$

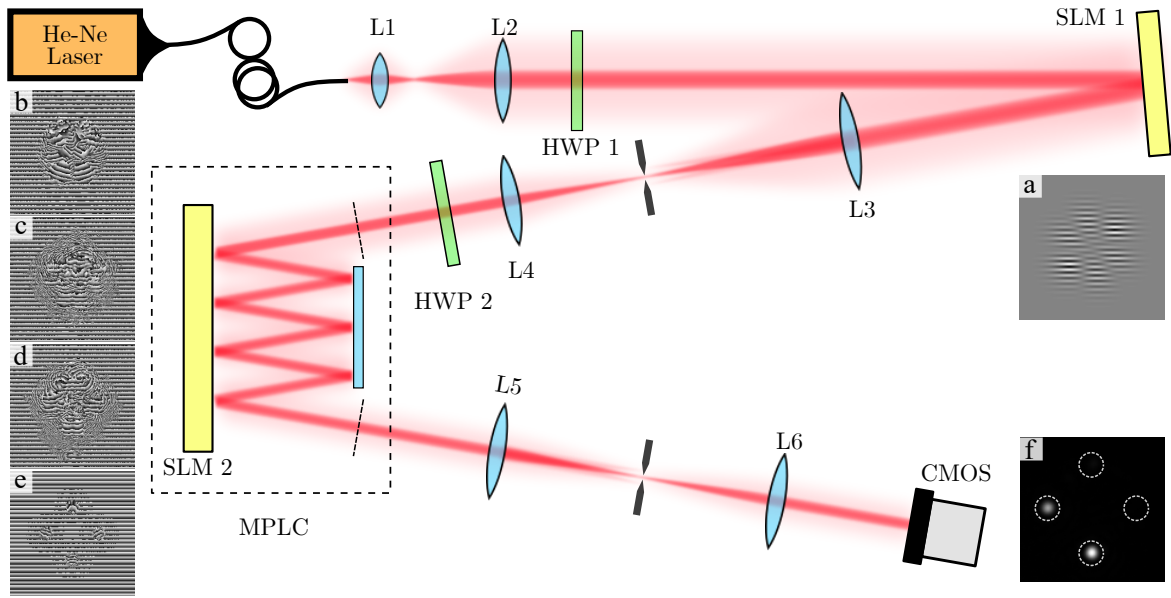


FIG. S.2. **Schematic of the experiment:** Input modes are generated using CGH holograms at SLM 1 (a). The light from SLM 1 is filtered and imaged to the MPLC where 4 phase masks with a constant grating (b-e) are displayed. The output modes of the MPLC are filtered and imaged to a CMOS camera where light is sorted into Gaussian spots (f). Lenses L1-6 have focal length 45mm, 100mm, 750mm, 500mm, 250mm and 250mm, respectively. HWP 1 and HWP 2 are half-wave plates.